Metal vs Ligand Reduction in Complexes of 1,3-Dimethylalloxazine (DMA) with Copper(I), Ruthenium(II), and Tungsten(VI). Crystal Structures of (DMA)WO_2Cl_2 and (Bis(1-methylimidazol-2-yl)ketone)WO_2Cl_2

Fridmann M. Hornung,[†] Oliver Heilmann,[†] Wolfgang Kaim,*[,†] Stanislav Zalis,[‡] and Jan Fiedler[‡]

Institut für Anorganische Chemie, Universität Stuttgart, Pfaffenwaldring 55, D-70550 Stuttgart, Germany, and J. Heyrovsky Institute of Physical Chemistry, Academy of Sciences of the Czech Republic, Dolejškova 3, CZ-18223 Prague, Czech Republic

Received February 18, 2000

The complexes [(DMA)Cu(PPh_3)$_2$](BF_4) (**1**) (DMA = 1,3-dimethylalloxazine), [(DMA)Ru(bpy)$_2$](PF_6)$_2$ (**2**), and (DMA)WO_2Cl_2 (**3**) were obtained as O^4-N^5-chelated species, as evident from an X-ray crystal structure analysis for **3** and from spectroscopy (NMR, IR, and UV−vis spectroelectrochemistry) for **1** and **2**. The tungsten(VI) center in **3** has its oxide ligands in a cis/equatorial position and the chloride ligands in a trans/axial position; it also exhibits a relatively short bond to O^4 (2.232(3) Å) and a very long bond to N^5 (2.462(3) Å). Comparison with the new structurally characterized compound (BIK)WO_2Cl_2 (**4**) (BIK = bis(1-methylimidazol-2-yl)ketone), which has W−N bonds of about 2.30 Å, confirms the unusual length of the W−N bond in **3**, probably caused by repulsion between one of the oxo ligands and the peri-hydrogen atom (H^6) of DMA. One-electron reduction of the complexes occurs reversibly at room temperature in THF (**1**, **2**) or at 198 K in CH_2Cl_2 (**3**). EPR spectroscopy reveals that this process is ligand-centered for **1** and **2** but metal-centered for **3**. Density functional methods and ab initio methodology are used to illustrate the correspondence in spin distribution between the radical anion π systems of alloxazine and isoalloxazine ("flavosemiquinone").

Introduction

The isoalloxazine chromophore of the flavin prosthetic group in flavin-containing oxidoreductases ("flavoenzymes") shows a two-step electron transfer behavior with an odd-electron "flavosemiquinone" as an intermediate.[1,2] Although flavoenzymes often contain metal centers,[3] including tungsten,[4] in suitable distances (<30 Å) for intraprotein electron transfer, a direct metal−flavin coordination has not yet been established in such enzymes. However, the capability of the isoalloxazine and related heterocycles to bind metal ions has long been recognized and was recently reviewed.[5] Biological electron transfer between flavin cofactors and metal centers[6] implies relatively close-lying potentials for the metal- and flavin-based redox pairs.

In this paper, we show through quantum chemical methods that the redox orbital of the 1,3-dimethylalloxazine (DMA) heterocyclic π system is closely related to that of the isoalloxazines of flavins.

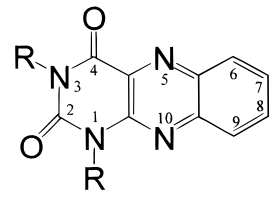

R = H alloxazine
R = CH_3 1,3-dimethylalloxazine (DMA)

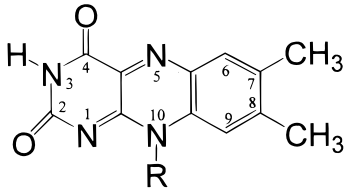

flavin structure

R = $CH_2[CH(OH)]_3CH_2OH$ riboflavin
R = CH_3 7,8,10-trimethylisoalloxazine (TMIA)

Using the DMA ligand in complexes [(DMA)Cu(PPh_3)$_2$](BF_4) (**1**), [(DMA)Ru(bpy)$_2$](PF_6)$_2$ (**2**, bpy = 2,2′-bipyridine), and (DMA)WO_2Cl_2 (**3**), we demonstrate that there are two alternatives for the electron transfer, viz., ligand- or metal-centered reduction processes. The complexes **1**−**3** are characterized by cyclic voltammetry, NMR, EPR, IR, UV−vis (spectro)electrochemistry, and, in the case of **3**, X-ray structural analysis. The unexpectedly long W−N bond of **3** prompted us to prepare,

[†] Universität Stuttgart.
[‡] Academy of Sciences of the Czech Republic.

(1) Fraaije, M. W.; Mattevi, A. *Trends Biochem. Sci.* **2000**, *25*, 126.
(2) (a) Walsh, C. T. *Acc. Chem. Res.* **1980**, *13*, 148. (b) Walsh, C. T. *Acc. Chem. Res*. **1986**, *19*, 216.
(3) (a) *Flavins and Flavoproteins*; Yagi, K., Ed.; de Gruyter: Berlin, 1994. (b) *Chemistry and Biochemistry of the Flavoenzymes*; Muller, F., Ed.; CRC Press: Boca Raton, FL, 1991.
(4) Hagen, W. R.; Arendsen, A. F. *Struct. Bonding (Berlin)* **1998**, *90*, 161.
(5) Kaim, W.; Schwederski, B.; Heilmann, O.; Hornung, F. *Coord. Chem. Rev.* **1999**, *182*, 323.
(6) Hemmerich, P.; Massey, V.; Michel, H.; Schug, C. *Struct. Bonding (Berlin)* **1982**, *48*, 93.

10.1021/ic0001816 CCC: $19.00
Published on Web 08/11/2000

crystallize, and study for comparison the compound (BIK)WO_2Cl_2 (**4**) (BIK = bis(1-methylimidazol-2-yl)ketone).

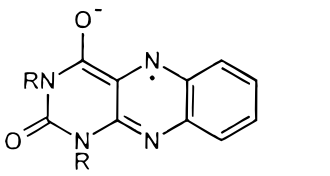

alloxazine radical anion
(R = CH_3: $DMA^{\bullet-}$)

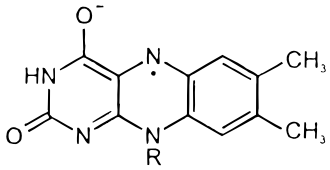

flavosemiquinone anion

Experimental Section

Instrumentation. EPR spectra were recorded in the X band on a Bruker System ESP 300 instrument equipped with a Bruker ER035M gaussmeter and a HP 5350B microwave counter. ^{1}H NMR spectra were taken on a Bruker AC 250 spectrometer, and infrared spectra were obtained using a Perkin-Elmer 684 spectrometer and a Paragon 1000 PC FTIR instrument. UV−Vis/NIR absorption spectra were recorded on spectrophotometers UV160 from Shimadzu and Omega 10 from Bruins Instruments. Cyclic voltammetry was carried out at a 100 mV/s standard scan rate in THF or dichloromethane/0.1 M Bu_4NPF_6 using a three-electrode configuration (glassy carbon electrode, Pt counter electrode, and Ag/AgCl reference), a PAR 273 potentiostat, and a function generator. The ferrocene/ferrocenium couple served as the internal reference. Spectroelectrochemical measurements were performed using an optically transparent thin-layer electrode (OTTLE) cell[7] for UV−vis spectra and a two-electrode capillary for EPR studies.[8] The reversibility of the processes was checked with the appearance of isosbestic points and the restoration of the starting spectra on reoxidation.

[(DMA)Cu(PPh$_3$)$_2$](BF$_4$) (1). A 40 mg (0.17 mmol) sample of DMA[9]was added under argon to a solution of 53.5 mg (0.17 mmol) of $[Cu(CH_3CN)_4](BF_4)$[10] in 25 mL of dry dichloromethane. Addition of 89.2 mg (0.34 mmol) of PPh_3 produced a red color. After being stirred for 30 min, the solution was first shock-frozen (77 K) and then allowed to thaw, upon which 25 mL of diethyl ether was added to produce an orange-brown precipitate. After standing at 280 K overnight, that precipitate was collected by filtration, redissolved in chloroform, reprecipitated by the addition of diethyl ether, collected again, and recrystallized from $CHCl_3$ to yield 130.8 mg (84%). Anal. Calcd for $C_{48}H_{40}BCuF_4N_4O_2P_2 \cdot CHCl_3$: C, 56.78; H, 3.99; N, 5.41. Found: C, 57.35; H, 4.02; N, 5.45.

[(DMA)Ru(bpy)$_2$](PF$_6$) (2). A solution of 40 mg (0.17 mmol) of DMA[9] and 88.5 mg (0.17 mmol) of $Ru(bpy)_2Cl_2 \cdot 2H_2O$ in 20 mL of ethylene glycol was treated with 154.4 mg (0.85 mmol) of KPF_6 in 3 mL of water. After being heated to reflux (90 min), the mixture turned to a purple-brown color; cooling the solution, adding 50 mL of water, and keeping the resulting mixture at 280 K overnight yielded a brown precipitate. Dissolution of the precipitate in 5 mL of acetone and reprecipitation with 20 mL of diethyl ether gave a greenish-brown material, which was washed with chloroform to remove free DMA. Recrystallization from 1,2-dichloroethane (DCE) yielded 38 mg (21%) of dark-green microcrystals. Anal. Calcd for $C_{32}H_{26}F_{12}N_8O_2P_2Ru \cdot 2DCE$: C, 37.82; H, 2.99; N, 9.80. Found: C, 35.74; H, 2.84; N, 9.98.

[(DMA)WO$_2$Cl$_2$] (3). A mixture of 128 mg (0.523 mmol) of DMA[9] and 150 mg (0.523 mmol) of $[WO_2Cl_2]_x$ was sealed in a glass ampule and heated to 520 K for 30 min. After being cooled, the brown product was dissolved in acetonitrile and filtered to remove any solid remains. The solvent was removed under vacuum from the filtrate to yield a yellowish product. Suspension of the product in 15 mL of dichloromethane and stirring the mixture for 24 h to dissolve any free DMA gave a yellow solution, which was cooled to 250 K to yield 97 mg (36%) of the yellow product. Anal. Calcd for $C_{12}H_{10}Cl_2N_4O_4W \cdot 2.5\ CH_2Cl_2$: C, 23.52; H, 2.04; N, 7.60. Found: C, 22.71; H, 1.68; N, 8.11.

[(BIK)WO$_2$Cl$_2$] (4). A mixture of 100 mg (0.526 mmol) of BIK[11] and 130 mg (0.453 mmol) of $[WO_2Cl_2]_x$ was suspended in 30 mL of dry DMF and stirred for 48 h at ambient temperature. The solvent was removed under vacuum, and the colorless residue was washed with 150 mL of warm acetonitrile to yield 179 mg (83%) of product **4**. Anal. Calcd for $C_9H_{10}Cl_2N_4O_3W$: C, 22.66; H, 2.11; N, 11.75. Found: C, 22.91; H, 2.11; N, 11.87.

Crystallography. Yellow crystals of (DMA)WO_2Cl_2 were obtained from dichloromethane at −20 °C. One single crystal (0.3 × 0.2 × 0.2 mm^3) was used for diffraction on a Syntex P2$_1$ diffractometer (Table 3): $4.94° < 2\theta < 60.02°$; $-16 \le h \le 15$, $-3 \le k \le 16$, $-16 \le l \le 16$; empirical absorption correction (ψ scan); 4737 collected and 4540 unique reflections; 209 parameters and no restraints.

Colorless platelets of (BIK)WO_2Cl_2 were obtained from acetonitrile at −20 °C. One single crystal (0.3 × 0.3 × 0.15 mm^3) was used for diffraction on a Siemens P4 diffractometer (Table 3): $4.00° \le 2\theta \le 56.04°$; $-19 \le h \le 19$, $-15 \le k \le 16$, $-4 \le l \le 18$; empirical absorption correction (ψ scan); 6522 collected and 3332 unique reflections; 188 parameters and no restraints.

The structures were solved by heavy-atom methods using the SHELXTL-PLUS[12] and SHELXL93 program packages (full-matrix least-squares methods for F^2).[13] Non-hydrogen atoms were refined anisotropically; hydrogen atoms were introduced at ideal positions and refined using the riding model.

Quantum Chemical Calculations. The electronic structures of DMA, TMIA, and their radical anions were examined through ab initio and density functional (DFT) methods.

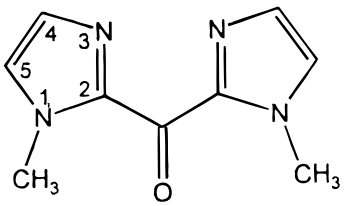

BIK

Calculations on radical anions were spin unrestricted. Calculations were performed using the GAUSSIAN98 program package.[14] Dunning's[15] valence double-ζ basis set with polarization functions was used for H, C, O, and N atoms. The B3LYP hybrid functional[16] was used within the DFT method. The calculations on neutral and reduced ligands were

(7) Krejcik, M.; Danek, M.; Hartl, F. *J. Electroanal. Chem.* **1991**, *317*, 179.
(8) Kaim, W.; Ernst, S.; Kasack, V. *J. Am. Chem. Soc.* **1990**, *112*, 173.
(9) (a) Mager, H. I. X.; Addink, R.; Berends, W. *Rec. Trav. Chim. Pays−Bas* **1967**, *86*, 833. (b) Bredereck, H.; Pfleiderer, W. *Chem. Ber.* **1954**, *87*, 1119.
(10) Hathaway, B. J.; Holah, D. G.; Postlethwaite, J. D. *J. Chem. Soc.* **1961**, 3215.
(11) Gorun, S. M.; Papaefthymiou, G. C.; Frankel, R. B.; Lippard, S. J. *J. Am. Chem. Soc.* **1987**, *109*, 4244.
(12) Sheldrick, G. M. *SHELXTL PLUS*; Siemens Analytical X-ray Instruments Inc.: Madison, WI, 1990.
(13) Sheldrick, G. M. *SHELXL93: Program for the Refinement of Crystal Structure*; University of Göttingen: Göttingen, Germany, 1993.
(14) Frisch, M. J.; Trucks, G. W.; Schlegel, H. B.; Scuseria, G. E.; Robb, M. A.; Cheeseman, J. R.; Zakrzewsik, V. G.; Montgomery, J. A., Jr.; Stratmann, R. E.; Burant, J. C.; Dapprich, S.; Millam, J. M.; Daniels, A. D.; Kudin, K. N.; Strain, M. C.; Farkas, O.; Tomasi, J.; Barone, V.; Cossi, M.; Cammi, R.; Mennucci, B.; Pomelli, C.; Adamo, C.; Clifford, S.; Ochterski, J.; Petersson, G. A.; Ayala, P. Y.; Cui, Q.; Morokuma, K.; Malick, D. K.; Rabuck, A. D.; Raghavachari, K.; Foresman, J. B.; Cioslowski, J.; Ortiz, J. V.; Stefanov, B. B.; Lium, G.; Liashenko, A.; Piskorz, P.; Komaromi, I.; Gomperts, R.; Martin, R. L.; Fox, D. J.; Keith, T.; Al-Laham, M. A.; Peng, C. Y.; Nanayakkara, A.; Gonzalez, C.; Challacombe, M.; Gill, P. M. W.; Johnson, B.; Chen, W.; Wong, M. W.; Andres, J. L.; Gonzalez, C.; Head-Gordon, M.; Replogle, E. S.; Pople, J. A. *Gaussian 98, Revision A.6*; Gaussian, Inc.: Pittsburgh, PA, 1998.
(15) Woon, D. E.; Dunning, T. H., Jr. *J. Chem. Phys.* **1993**, *98*, 1358.

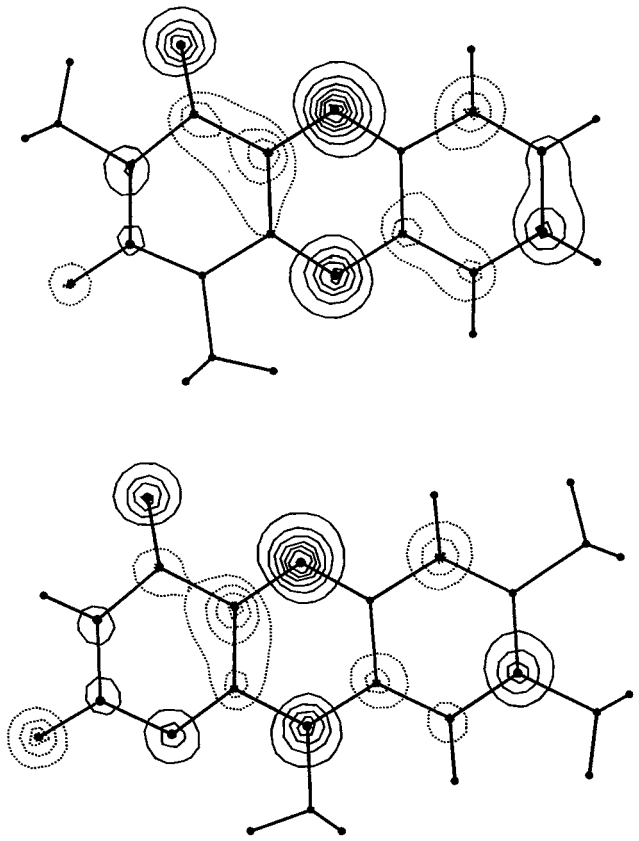

Figure 1. DFT-calculated contour maps of the a″ SOMO of DMA$^{\bullet-}$ (top) and TMIA$^{\bullet-}$ (bottom), 0.5 Å above the molecular plane. Full lines for positive contour values and dashed lines for negative contour values.

done within approximate planar configurations (C_s symmetry). The results correspond to the geometry-optimized structures.

Results and Discussion

Comparison of Alloxazine and Isoalloxazine Redox Orbitals. Although there has been a number of quantum chemical calculations of flavins and their reduced forms,[17] we have now employed spin-unrestricted DFT methods for a direct comparison of the "redox orbitals" of DMA and the 7,8,10-trimethylisoalloxazine (TMIA) ring system of the flavins. That redox orbital (π^*) is the lowest unoccupied molecular orbital (LUMO) of the unreduced forms and the singly occupied molecular orbital (SOMO) of the one-electron reduced, i.e., radical species.

As Figure 1 illustrates, the π^* MOs of a″ symmetry look very similar, centered mainly on the nitrogen atoms N^5 and N^{10} of the central pyrazine rings and on O^4. The use of ab initio methods yielded essentially the same result. Calculated spin densities on N^5 are 0.367 and 0.352 for DMA$^{\bullet-}$ and TMIA$^{\bullet-}$, respectively; the corresponding figures on N^{10} are 0.163 and 0.099. Thus, from the point of spin distribution, the DMA radical anion is a reasonably good model for flavosemiquinones.

Synthesis and Spectroscopic Characterization. The complexes **1**−**3** were obtained from DMA and precursor complexes along standard routes.[18−20] The question of the metal binding site can be approached using ^{1}H NMR and IR spectroscopy: The standard O^4-N^5 coordination of such ligands (i.e., lumazines, pterins, alloxazines, flavins[5,21−23]) manifests itself through low-field shifts of the ring protons of the heterocycle (Table 1) and through the low-energy shift of the $\nu_{C^4=O}$ carbonyl stretching band. In contrast, the $\nu_{C^2=O}$ band shows less pronounced effects. The data listed in Table 2 confirm this expectation, which is further substantiated through a structural analysis of complex **3** (cf. below). Further evidence for the binding of π-electron-rich Cu^I (**1**) and Ru^{II} (**2**) metal centers to the $O^4-C^4-C^5-N^5$ π-acceptor site of DMA comes from intense metal-to-ligand charge transfer (MLCT, $d_\pi \rightarrow \pi^*$) absorptions in the visible part of the spectrum (cf. Figure 8 and Table 8), which is similarly known for other complexes with $[Cu(PPh_3)_2]^+$ [18,24] or $[Ru(bpy)_2]^{2+}$ fragments[19,25] with chelating π-acceptor ligands. The W^{VI} complex, in contrast, does not exhibit long-wavelength bands in the visible region; DMA itself has a characteristic narrow band at about 380 nm, which also appears in the spectra of the complexes (Figure 8).[26]

Table 1. ^{1}H NMR Data of DMA Complexes[a]

compound	solvent	N^3-CH_3	N^1-CH_3	H^6	H^7	H^8	H^9
DMA	CD_3CN	3.46	3.73	8.22	7.81	7.95	8.03
1[c]	$(CD_3)_2CO$	3.56	3.80	7.71			8.21[b]
2[d]	$(CD_3)_2CO$	3.57	3.82	7.99			8.71[b]
3	CD_3CN	3.74	3.85	9.70	8.17	8.32	8.28
3	CD_2Cl_2	3.85	3.95	9.78	8.12	8.22	8.31

[a] Multiplicity: N^3-CH_3, N^1-CH_3 (s); H^6, H^9 (d); H^7, H^8 (m). [b] Multiplet structure, higher-order spectra. [c] Phenyl protons of $P(PPh_3)_3$ groups at 7.35−7.57 ppm. [d] Pyridyl protons of bpy coligands at 6.97−8.92 ppm.

Table 2. Carbonyl Stretching Vibrations $\nu_{C=O}$ (cm^{-1}) of DMA Complexes

compound	$\nu_{C^2=O}$	$\nu_{C^4=O}$	medium
DMA	1712s	1681m	CH_2Cl_2
DMA	1721s	1668s	Nujol
1	1727s	1653vs	CH_2Cl_2
1$^{\bullet-}$	1679s[b]	1590m	CH_2Cl_2
2	1727s	1614vs	CH_2Cl_2
2	1727s	1617vs	CH_3CN
2$^{\bullet-}$	1686s	1596w	CH_3CN
3[a]	1735s	1634s	Nujol

[a] $\nu_{W=O}$ at 978 and 930 cm^{-1}. [b] Low-energy shoulder.

Crystal Structure of 3. Single crystals of **3** could be obtained from a solution in CH_2Cl_2 at 253 K. The results from the X-ray diffraction analysis (Table 3) are summarized in Table 4, and Figure 2 illustrates the molecular structure. (Note the discrepancy between the superscript numbering according to heterocyclic nomenclature[5] and the numbering from the crystal structure analysis.)

The tungsten(VI) atom in **3** exhibits a distorted octahedral coordination sphere; the metal is coordinated in a familiar fashion[5] by the O^4-N^5 atoms O3 and N1 of the heterocycle.

(16) Stephens, P. J.; Devlin, F. J.; Cabalowski, C. F.; Frisch, M. J. *J. Phys. Chem.* **1994**, *98*, 11623.
(17) (a) Edmondson, D. E.; Tollin, G. *Top. Curr. Chem.* **1983**, *108*, 109. (b) Kurrek, H.; Bock, M.; Bretz, N.; Elsner, M.; Kraus, H.; Lubitz, W.; Möller, F.; Geissler, J.; Kroneck, P. M. H. *J. Am. Chem. Soc.* **1984**, *106*, 737.
(18) (a) Kaim, W.; Kohlmann, S. *Inorg. Chem.* **1987**, *26*, 1469. (b) Bessenbacher, C.; Ernst, S.; Kohlmann, S.; Kaim, W.; Kasack, V.; Roth, E.; Jordanov, J. *J. Chem. Soc., Faraday Trans. 1* **1989**, *85*, 4075.
(19) Ernst, S.; Hänel, P.; Jordanov, J.; Kaim, W.; Kasack, V.; Roth, E. *J. Am. Chem. Soc.* **1989**, *111*, 1733.
(20) Hornung, F.; Kaim, W. *J. Chem. Soc., Faraday Trans.* **1994**, *90*, 2909.
(21) Huesco-Ureña, F.; Jiménez-Pulido, S. B.; Moreno-Carretero, M. N.; Quirós-Olozábal, M.; Salas-Peregrín, J. M. *Polyhedron* **1999**, *18*, 85.
(22) Kaufmann, H. L.; Carroll, P. J.; Burgmayer, S. J. N. *Inorg. Chem.* **1999**, *38*, 2600.
(23) (a) Fischer, B.; Schmalle, H.; Dubler, E.; Schäfer, A.; Viscontini, M. *Inorg. Chem.* **1995**, *34*, 5726. (b) Kaufmann, H. L.; Liable-Sands, L.; Rheingold, A. L.; Burgmayer, S. J. N. *Inorg. Chem.* **1999**, *38*, 2592.
(24) Vogler, C.; Kaim, W. *Z. Naturforsch.* **1992**, *47b*, 1057.
(25) Ernst, S. D.; Kaim, W. *Inorg. Chem.* **1989**, *28*, 1520.
(26) Heilmann, O.; Hornung, F.; Kaim, W.; Fiedler, J. *J. Chem. Soc., Faraday Trans.* **1996**, *92*, 4233.

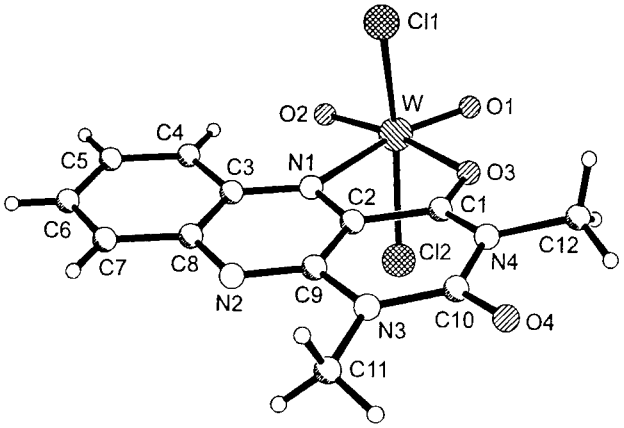

Figure 2. Molecular structure of **3** in the crystal with atom numbering.

Table 3. Crystallographic Data for Complexes **3** and **4**

empirical formula	$C_{12}H_{10}Cl_2N_4O_4W$	$C_9H_{10}Cl_2N_4O_3W$
formula weight	528.99	476.96
space group	$P2_1/n$	*Pnma*
T (K)	183	183
a (Å)	11.408(3)	15.106(3)
b (Å)	11.785(3)	12.663(3)
c (Å)	11.579(2)	13.838(3)
β (deg)	90.92(2)	90
V (Å^3)	1556.5(6)	2647.0(1)
Z	4	8
ρ_{calc} (g cm^{-3})	2.257	2.394
λ (Å)	0.71073	0.71073
μ (mm^{-1})	7.789	9.140
R[a]	0.0315	0.0426
Rw[b]	0.0866	0.1025

[a] $R = (\Sigma||F_o| - |F_c||)/\Sigma|F_o|$. [b] $Rw = \{\Sigma[w(|F_o|^2 - |F_c|^2)^2]/\Sigma[w(F_o^4)]\}^{1/2}$.

Table 4. Selected Bond Lengths (Å) and Angles (deg) for **3**

W−O3	2.232(3)	W−N1	2.462(3)
W−O1	1.697(3)	W−O2	1.715(3)
W−Cl1	2.3480(12)	W−Cl2	2.3404(11)
C3−N1	1.361(5)	N1−C2	1.323(5)
C2−C1	1.457(5)	C1−O3	1.248(4)
C1−N4	1.337(5)	C10−O4	1.200(5)
O3−W−N1	69.57(10)	Cl1−W−Cl2	156.14(4)
O1−W−O2	104.3(2)	W−N1−C2	111.9(2)
O1−W−O3	90.8(2)	N1−C2−C1	116.5(3)
O2−W−N1	95.35(13)	C2−C1−O3	120.5(3)

Scheme 1

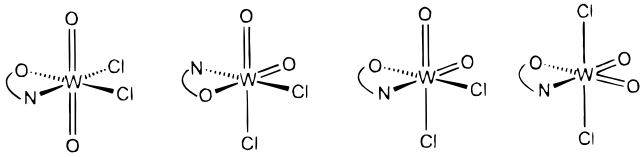

Of the various positional isomers in Scheme 1, the last alternative is realized in which the oxide ligands lie in the plane of the chelate ring and the chloride ligands are situated in the axial positions. The small-bite O3−W−N1 angle of 69.6(1)° stands in contrast to the 104.3(2)° for the cis dioxo group O1−W−O2. There is also a significant deviation of the Cl1−W−Cl2 angle at 156.14(4)° from linearity in the axis—a typical effect of bending away from the cis dioxometal angle.

In comparison to free alloxazine ligands,[27] complex **3** exhibits a shortening of the C1−O3 distance by about 0.03 Å through coordination. The DMA ligand experiences a slight distortion toward a boat-type structure with same-sign deviations for the atoms C1, C4, C7, and N3 from the mean plane. The angles between six-membered rings are small at 7.1(2)° (pyrimidinedione/pyrazine) and 2.6(3)° (pyrazine/benzene).

The bonds from the metal to the chelate donor centers are remarkably different: The W−N1 distance is much longer at 2.462(3) Å than the W−O3 bond at 2.232(3) Å. Although the latter is still very different from the oxotungsten(VI) bonds at about 1.70 Å, it is clear, especially by comparison of related structures,[5] that the "hard" W^{VI} center prefers bonding to the oxygen donor in the DMA chelate arrangement. Apparently, this center is better for largely electrostatic interactions than the nitrogen alternative (which, however, offers a better opportunity for π back-donation from more electron-rich metal centers, as illustrated by Figure 1). Another effect disfavoring bonding between W and N1 is the close contact between the peri-hydrogen atom of H−(C4) and the oxo atom O2 at about 2.38 Å, which pushes the metal fragment toward the oxygen donor part of the DMA chelate. Such a repulsive interaction is absent in complexes of lumazines[20] (without peri-hydrogen atoms) and in the structurally characterized DMA complex $[(DMA)IrCl(\eta^5\text{-}C_5Me_5)](PF_6)$,[28] where the approximately tetrahedral configuration at the metal precludes such close contact. The structural result explains the unusually strong low-field ^{1}H NMR shift of the peri-proton (H^6 in Table 1); on the other hand, the $\nu_{W=O}$ stretching frequencies seem little affected (Table 2).

To further evaluate this long W−N1 bond, we prepared and crystallized the compound $(BIK)WO_2Cl_2$ (**4**); BIK is a frequently used ligand in bioinorganic coordination chemistry.[11,29−31]

Table 2 contains crystallographic information of **4**, and Table 5 contains its selected bond parameters. Figure 3 illustrates the structure of the two crystallographically independent molecules.

Despite the hardness of W^{VI}, the coordination of WO_2Cl_2 to BIK occurs through the nitrogen atoms and not via the oxygen atom. Compound **4** exhibits a "type I" [32] intermolecular Cl···

Table 5. Selected Bond Lengths (Å) and Angles (deg) for **4**

molecule 1		molecule 2	
W1−O12	1.723(5)	W2−O22	1.743(5)
W1−N11	2.316(6)	W2−N21	2.294(6)
W1−Cl11	2.350(3)	W2−Cl21	2.351(3)
W1−Cl12	2.349(3)	W2−Cl22	2.371(3)
N11−C11	1.314(9)	N21−C21	1.343(8)
C11−C15	1.487(8)	C21−C25	1.481(8)
C15−O11	1.203(13)	C25−O21	1.180(13)
N11−W1−N11[a]	77.0	N21−W2−N21[a]	78.4(3)
O12−W1−O12[a]	104.8(3)	O22−W2−O22[a]	104.6(4)
O12−W1−N11	89.1(2)	O22−W2−N21	88.5(2)
Cl11−W1−Cl12	158.68(10)	Cl21−W2−Cl22	159.90(13)
W1−N11−C11	133.9(5)	W2−N21−C21	133.4(5)
N11−C11−C15	127.4(7)	N21−C21−C25	127.8(6)
C11−C15−C11[a]	118.3(8)	C21−C25−C21[a]	119.1(8)

[a] Transformation for symmetrically equivalent atoms "a": x, $^1/_2 - y$, z.

(27) (a) Csöregh, I.; Kierkegaard, P.; Koziol, J.; Müller, F. *Acta Chem. Scand.* **1987**, *B41*, 383. (b) Kumar, V.; Wood, K. A.; Bryan, R. F.; Averill, B. A. *J. Am. Chem. Soc.* **1986**, *108*, 490.

(28) Heilmann, O.; Hornung, F.; Fiedler, J.; Kaim, W. *J. Organomet. Chem.* **1999**, *589*, 2.

(29) (a) Grehl, M.; Krebs, B. *Inorg. Chem.* **1994**, *33*, 3877. (b) Reusmann, G.; Grehl, M.; Reckordt, W.; Krebs, B. *Z. Anorg. Allg. Chem.* **1994**, *620*, 199.

(30) (a) Byers, P. K.; Canty, A. J.; Engelhardt, L. M.; Patrick, J. M.; White, A. H. *J. Chem. Soc., Dalton Trans.* **1985**, 981. (b) Chen, X.-M.; Xu, Z.-T.; Mak, T. C. W. *Polyhedron* **1995**, *35*, 1295.

(31) Stange, A. F.; Kaim, W. *Z. Anorg. Allg. Chem.* **1996**, *622*, 1118.

(32) Pedireddi, V. R.; Reddy, D. S.; Goud, B. S.; Craig, D. C.; Rae, A. D.; Desiraju, G. R. *J. Chem. Soc., Perkin Trans.* **1994**, 2353.

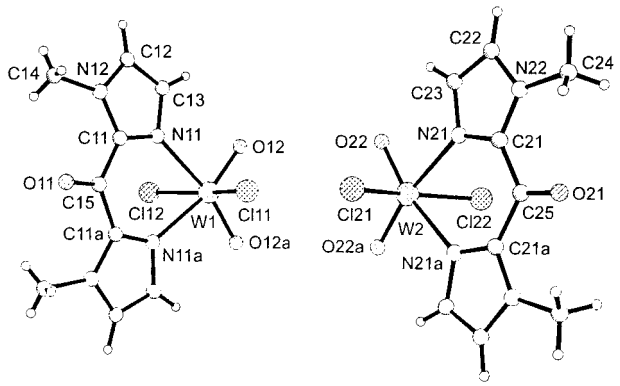

Figure 3. Structures of the two crystallographically independent molecules of **4** in the crystal with atom numbering.

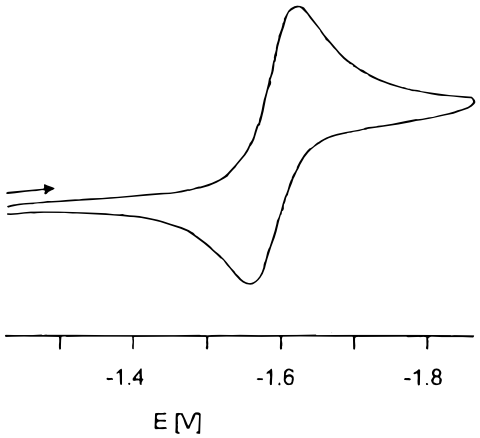

Figure 4. Cyclic voltammogram of **3** at 198 K in CH_2Cl_2/0.1 M Bu_4NPF_6 (100 mV/s scan rate, potentials vs $(C_5H_5)_2Fe^{+/0}$).

Table 6. Electrochemical Potentials of DMA Complexes[a]

compound	*E*(red 1)	*E*(red 2)	*E*(red 3)	*E*(red 4)
DMA	−1.65	−2.33[b]		
1	−1.00	−1.87[b]		
2[c]	−0.79	−1.67	−2.13	−2.48
3[d]	−1.59			

[a] From cyclic voltammetry at 100 mV/s scan rate in THF/0.1 M Bu_4NPF_6, unless noted otherwise. Potentials in V vs $(C_5H_5)_2Fe^{+/0}$; half-wave potentials, unless stated otherwise. [b] Cathodic peak potential for the irreversible process. [c] Oxidation at $E_{1/2}$(ox 1) = 0.95 V. [d] At 198 K in CH_2Cl_2/0.1 M Bu_4NPF_6.

Cl interaction between Cl21 and Cl12 at 3.343 Å, which is similarly observed for Cl_2 and other compounds. The general bonding pattern of both crystallographically independent molecules in the crystal of **4** is very similar to those described for **3** and $(bpy)WO_2Cl_2$.[33] The W−N bonds of about 2.30 Å are in the normal range for **4**, confirming that **3** exhibits an unusually elongated W−N bond.

Cyclic Voltammetry. All three complexes **1**−**3** undergo electrochemical reduction at readily accessible potentials. Whereas **1** shows one reversible wave, **2** exhibits four reversible processes at room temperature in THF[5] (Table 6). The tungsten(VI) compound **3**, however, shows reversible electron uptake only at low temperature; Figure 4 illustrates the cyclic voltammogram of **3** at 198 K in CH_2Cl_2. In agreement with the results from EPR spectroscopy, the lack of reversibility for the transition **3** → **3**$^{\bullet-}$ is attributed to the metal-centered reduction W^{VI} → W^{V}, which is likely to cause the dissociative labilization of chloride—a behavior well known for other reduced transition metal halides.[34,35] The additional reversible reduction processes for **2** at negative potentials are attributed to the second reduction of DMA,[26] according to the general Scheme 2 for α-iminocarbonyl chelate redox systems, and the expected reduction of the bpy coligands (cf. below).[25] Although the conditions of measurement are somewhat different, the potentials of the first electron uptake clearly become less negative along the sequence **3** < **1** < **2**, which also correlates with increasing reversibility.

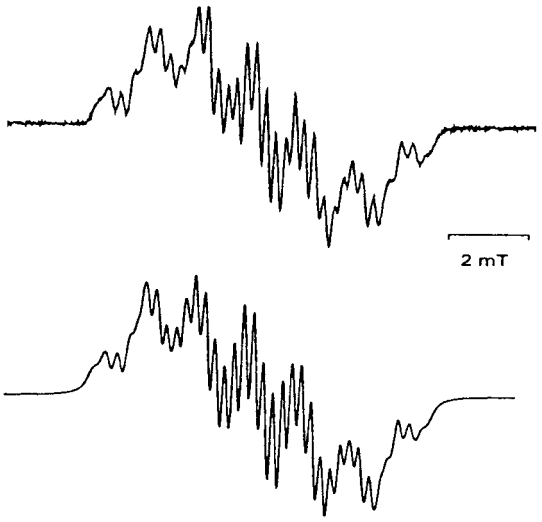

Figure 5. EPR spectrum of **1**$^{\bullet-}$ (top) in THF/0.1 M Bu_4NPF_6 with computer simulation (bottom, 0.22 mT line width).

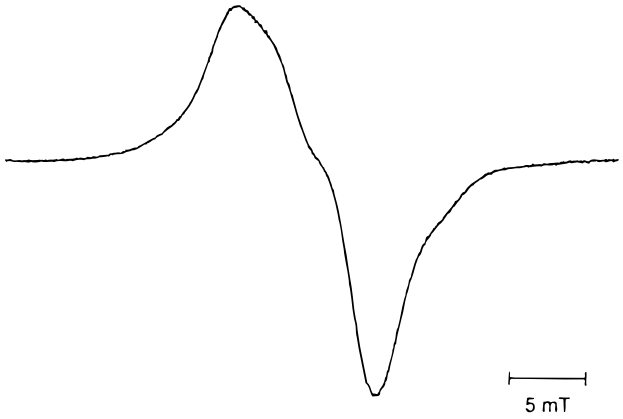

Figure 6. EPR spectrum of **3**$^{\bullet-}$ at 4 K in CH_2Cl_2/0.1 M Bu_4NPF_6.

Scheme 2

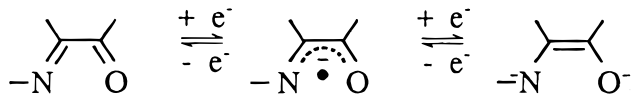

EPR Spectroscopy. The most direct evidence for the difference between complexes **1** and **2** with ligand-centered reduction and compound **3** with metal-based electron uptake comes from the EPR spectra of the one-electron reduced forms, as obtained by in situ electrolysis (Figure 5).

Reduced **1** and **2** show spectra with the hyperfine structure dominated by the ^{14}N atom in position N^5 (Figure 6); ^{31}P (**1**$^{\bullet-}$) and metal isotope hyperfine coupling (^{63}Cu, $I = {}^3/_2$, 69.09% natural abundance; ^{65}Cu, $I = {}^3/_2$, 30.91%; ^{99}Ru, $I = {}^5/_2$, 12.72%;

(33) Herrmann, W. A.; Thiel, W. R.; Herdtweck, E. *Chem. Ber.* **1990**, *123*, 271.
(34) Klein, A.; Vogler, C.; Kaim, W. *Organometallics* **1996**, *15*, 236.
(35) Ladwig, M.; Kaim, W. *J. Organomet. Chem.* **1991**, *419*, 233.

Table 7. EPR Data of Reduced DMA Complexes[a]

compound	g	$a(N^5)$	$a(N^{10})$	$a(H^6)$	$a(H^9)$	a(M)	solvent
$DMA^{\bullet-}$	2.0035	0.64	0.33	0.33	0.33	−	THF
$\mathbf{1}^{\bullet-}$ [b]	2.0038	0.74	0.28	0.28	0.28	1.29(^{65}Cu) 1.21(^{63}Cu)	THF
$\mathbf{2}^{\bullet-}$	1.9990	0.80	not resolved			0.53(^{101}Ru) 0.47(^{99}Ru)	THF
$\mathbf{3}^{\bullet-}$ [c]	1.81 (g_1) 1.78 (g_2) 1.76 (g_3)	not resolved					CH_2Cl_2

[a] From in situ electrolysis in 0.1 M Bu_4NPF_6 solutions. Coupling constants in mT. [b] $a(^{31}P) = 1.02$ mT. [c] Electrolysis at 198 K, EPR measurements at 4 K.

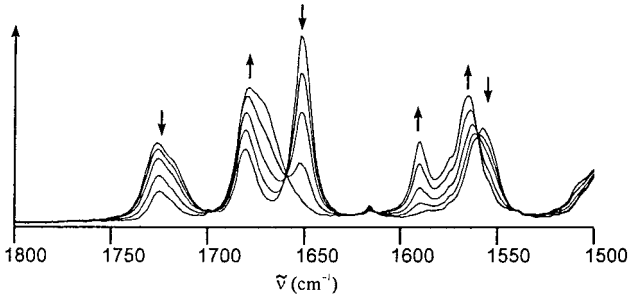

Figure 7. IR spectroelectrochemical reduction of **1** in THF/0.1 M Bu_4NPF_6.

^{101}Ru, $I = {}^5/_2$, 17.07%) is detectable but relatively small (Table 7).[18,19] Similar values corresponding to $a/a_o < 10^{-3}$ (a_o = isotropic hyperfine constant[36]) have been observed for related complexes such as $[(DMA)Re(CO)_3Cl]^{\bullet-}$, $[(DMA)IrCl(\eta^5\text{-}C_5Me_5)]^{\bullet}$, $[(L)Ru(bpy)_2]^{\bullet+}$, and $[(L)Cu(PPh_3)_2]^{\bullet}$.[8,24,28] In the case of reduced **1**, we could detect further DMA-centered hyperfine coupling (Figure 5, Table 7). The isotropic g values (Table 7) of $[(DMA)Cu(PPh_3)_2]^{\bullet}$ and $[(DMA)Ru(bpy)_2]^{\bullet+}$ confirm this assignment through the closeness to $g = 2.0035$ of the free-ligand radical anion.[28]

One-electron reduced **3**, on the other hand, exhibits a typical W^V EPR signal[20,37] in the glassy frozen state with g components at $g_1 = 1.81$, $g_2 = 1.78$, and $g_3 = 1.76$; one shoulder, presumably from ^{183}W isotope coupling (^{183}W, $I = {}^1/_2$, 14.3%), is visible at the high-field side.

Obviously, the reduction occurs at the high-valent metal and not at the DMA π-acceptor ligand, in full agreement with the reactivity of that anionic form at $T > 200$ K, as illustrated by the irreversible electrochemical response.

IR and UV−Vis Spectroelectrochemistry. An alternative to EPR in determining the site of electron transfer in coordination compounds is spectroelectrochemistry in the UV−vis and IR regions. This method is also applicable to diamagnetic states or intermediates which do not exhibit useful EPR signals. Using an optically transparent thin-layer electrochemical (OTTLE) cell, we first studied reversibly reducible **1** and **2** in the carbonyl stretching region of the infrared.

Figure 7 illustrates the effect of one-electron uptake by **1** on the carbonyl stretching bands of coordinated DMA; Table 2 contains the pertinent data.

It is obvious that the EPR spectroscopically established reduction of the coordinated DMA ligand is reflected by a low-field shift of both $\nu_{C=O}$ bands and by a particular intensity decrease of $\nu_{C^2=O}$.[28] The low-field shift results from decreased C−O bond orders, similarly observed for the 1,2-dioxolene (*o*-quinone) redox series;[38] the intensity reduction for the non-coordinated carbonyl function has been noted before.[28] Infrared bands belonging to vibrations which are less affected by the occupation of the redox orbital (Figure 1) exhibit only marginal shifts; Figure 7 illustrates one such feature ($\nu_{C=C}$ or $\nu_{C=N}$) changing from 1567 to 1559 cm^{-1}.

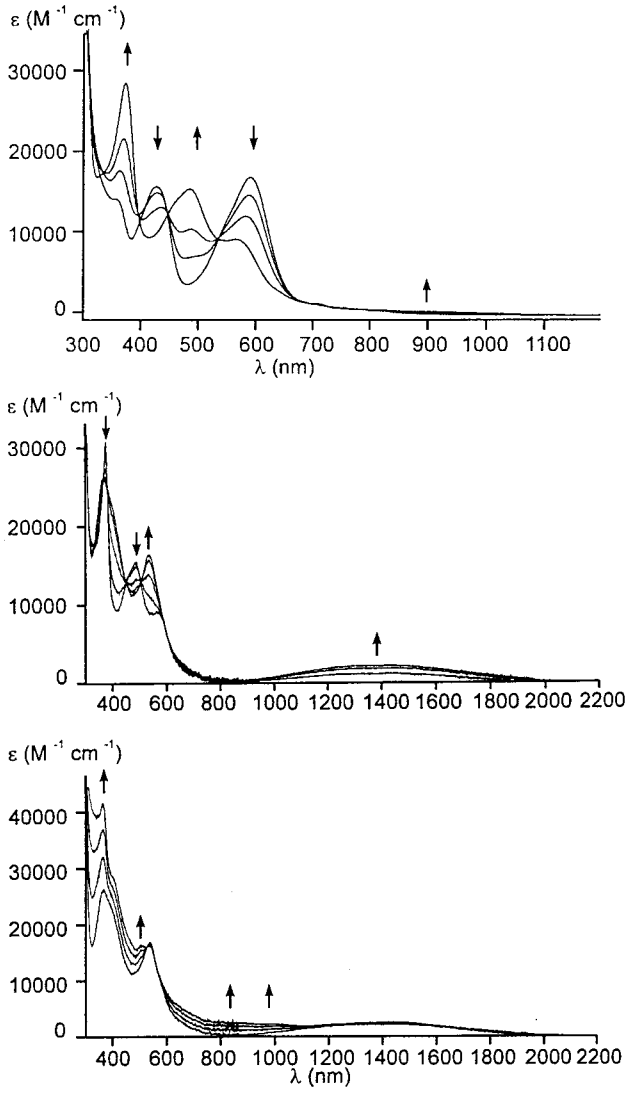

Figure 8. UV−vis spectroelectrochemical reduction of **2** to $\mathbf{2}^{\bullet-}$ (top), $\mathbf{2}^{2-}$ (center), and $\mathbf{2}^{3-}$ (bottom) in THF/0.1 M Bu_4NPF_6.

Spectroelectrochemistry in the UV−vis region is particularly interesting for the multiply reducible system **2**, where the sequence of electron acquisition after the first reduction of DMA is not immediately obvious. Figure 8 shows the corresponding results for $\mathbf{2}^n$, and Table 8 summarizes all UV−vis/NIR absorption data.

The low-energy MLCT bands for the transitions $d_\pi(M) \rightarrow \pi^*(DMA)$ of **1** at 470 nm and of **2** at 593 nm are diminished and hypsochromically shifted on one-electron reduction. Instead, weak intraligand transitions for $DMA^{\bullet-}$ appear at $\lambda > 550$ nm[26,28], and the $d_\pi(M) \rightarrow \pi^*(bpy)$ transitions are bathochromically shifted.[25] Another feature, which is particular for $\mathbf{2}^{\bullet-}$

(36) Weil, J. A.; Bolton, J. R.; Wertz, J. E. *Electron Paramagnetic Resonance*; Wiley: New York, 1994.
(37) (a) Collison, D.; Garner, C. D.; Joule, J. A. *Chem. Soc. Rev.* **1996**, 25. (b) Goodman, B. A.; Raynor, J. B. *Adv. Inorg. Chem. Radiochem.* **1970**, *13*, 135.
(38) (a) Haga, M.; Dodsworth, E. S.; Lever, A. B. P. *Inorg. Chem.* **1986**, *25*, 447. (b) Lever, A. B. P.; Auburn, P. R.; Dodsworth, E. S.; Haga, M.; Liu, W.; Melnik, M.; Nevin, W. A. *J. Am. Chem. Soc.* **1988**, *110*, 8076.

Table 8. Absorption Data of DMA Complexes

compound	λ_{max} (log ϵ)[a]	solvent
DMA	319(3.96), 364sh, 378(4.03), 393sh	THF
DMA	320, 361sh, 381, 398sh	CH_3CN
1	352(4.00), 404(3.92), 420sh, 470(3.62)	CH_2Cl_2
$\mathbf{1}^{\bullet-}$	323(4.03), 380(4.17), 470(3.44), 665(2.56)	CH_2Cl_2
2	362(4.15), 399sh, 421(4.19), 435(4.18), 593(4.23)	CH_3CN
$\mathbf{2}^{\bullet-}$	378(4.49), 490(4.19), 564(3.96), 920(2.27)	CH_3CN
$\mathbf{2}^{2-}$	378(4.42), 419sh, 535(4.21), 1430(3.33)	CH_3CN
$\mathbf{2}^{3-}$	378(4.62), 419sh, 513(4.21), 535(4.21), 882 (3.37), 998(3.37), 1430(3.42)	CH_3CN
3	319, 358sh, 380, 400sh	CH_3CN

[a] λ_{max} in nm, ϵ in M^{-1} cm^{-1}.

(at 920 nm) and becomes more prominent for $\mathbf{2}^{2-}$ at 1430 nm, is the ligand-to-ligand charge transfer (LLCT) transitions from singly or doubly reduced DMA to the π-accepting 2,2′-bipyridine coligands. These bands are usually broad and well known from the spectroelectrochemistry of $[Ru(bpy)_2]^{2+}$ complexes of *o*-quinonoid ligands.[38] The third reduction appears to occur at one of the coordinated bpy ligands, leaving the LLCT little changed but showing added weak bands around 800−900 nm (LLCT of $bpy^{\bullet-}$).[38,39]

In summary, we have demonstrated that the DMA ligand is a convenient substitute for the metal-binding flavin π system and that metal- or ligand-centered reduction can occur, depending on the nature of the metal complex fragment. In the present situation, the cationic but π-electron-rich copper(I) and ruthenium(II) complex fragments with metals in rather low oxidation states cause the reduction of the heterocyclic ligand, whereas the coordination of the WO_2Cl_2 fragment with high-valent metal and conspicuously weak W−N binding leads to the primary electron acquisition by the metal. A correlation between the M−N bond length and the metal vs ligand oxidation state alternative has been similarly established for metallopterins,[22,23,40,41] with which the alloxazine system shares some common structural and electronic features.

Acknowledgment. The authors thank Deutsche Forschungsgemeinschaft (Schwerpunktprogramm "Bioinorganic Chemistry") and Volkswagenstiftung (Schwerpunktprogramm "Electron Transfer") and the Ministry of Education of the Czech Republic (OC.D14.20).

Supporting Information Available: Two crystallographic files in CIF format for compounds **3** and **4**. This material is available free of charge via the Internet at http://pubs.acs.org.

IC0001816

(39) Krejcik, M.; Zalis, S.; Ladwig, M.; Matheis, W.; Kaim, W. *J. Chem. Soc., Perkin Trans. 2* **1992**, 2007.

(40) Burgmayer, S. J. N. *Struct. Bonding (Berlin)* **1998**, *92*, 67.

(41) (a) Kaufmann, H. L.; Liable-Sands, L.; Rheingold, A. L.; Burgmayer, S. J. N. *Inorg. Chem.* **1999**, *38*, 2592. (b) Kaufmann, H. L.; Carroll, P. J.; Burgmayer, S. J. N. *Inorg. Chem.* **1999**, *38*, 2600. (c) Burgmayer, S. J. N.; Kaufmann, H. L.; Fortunato, G.; Hug, P.; Fischer, B. *Inorg. Chem.* **1999**, *38*, 2607.